Topological properties and fractal analysis of a recurrence network constructed from fractional Brownian motions

Jin-Long Liu,[1] Zu-Guo Yu,[1,2,*] and Vo Anh[2]

[1]*Hunan Key Laboratory for Computation and Simulation in Science and Engineering and Key Laboratory of Intelligent Computing and Information Processing of Ministry of Education, Xiangtan University, Xiangtan, Hunan 411105, China*

[2]*School of Mathematical Sciences, Queensland University of Technology, GPO Box 2434, Brisbane, Q4001, Australia*

Many studies have shown that we can gain additional information on time series by investigating their accompanying complex networks. In this work, we investigate the fundamental topological and fractal properties of recurrence networks constructed from fractional Brownian motions (FBMs). First, our results indicate that the constructed recurrence networks have exponential degree distributions; the average degree exponent $\langle \lambda \rangle$ increases first and then decreases with the increase of Hurst index H of the associated FBMs; the relationship between H and $\langle \lambda \rangle$ can be represented by a cubic polynomial function. We next focus on the motif rank distribution of recurrence networks, so that we can better understand networks at the local structure level. We find the interesting superfamily phenomenon, i.e., the recurrence networks with the same motif rank pattern being grouped into two superfamilies. Last, we numerically analyze the fractal and multifractal properties of recurrence networks. We find that the average fractal dimension $\langle d_B \rangle$ of recurrence networks decreases with the Hurst index H of the associated FBMs, and their dependence approximately satisfies the linear formula $\langle d_B \rangle \approx 2 - H$, which means that the fractal dimension of the associated recurrence network is close to that of the graph of the FBM. Moreover, our numerical results of multifractal analysis show that the multifractality exists in these recurrence networks, and the multifractality of these networks becomes stronger at first and then weaker when the Hurst index of the associated time series becomes larger from 0.4 to 0.95. In particular, the recurrence network with the Hurst index $H = 0.5$ possesses the strongest multifractality. In addition, the dependence relationships of the average information dimension $\langle D(1) \rangle$ and the average correlation dimension $\langle D(2) \rangle$ on the Hurst index H can also be fitted well with linear functions. Our results strongly suggest that the recurrence network inherits the basic characteristic and the fractal nature of the associated FBM series.

PACS number(s): 89.75.Hc, 05.45.Df, 47.53.+n

I. INTRODUCTION

Methods of nonlinear time series analysis have been widely applied in physics, physiology, finance, and biology. Complex network theory has become one of the most important developments in statistical physics [1]. Recent studies have shown that complex network theory may be an effective method to extract the information embedded in time series [2,3]. Many complicated dynamics systems in nature and society can be described by complex networks. In a complex system, its elements are represented by nodes, and their interactions are represented by directed or undirected edges.

Based on the small-world and scale-free properties of complex networks [4,5], Newman *et al.* [6] investigated extensively the structure and function of real-world complex networks in different areas. The advancement of network theory provides us with another perspective to perform time series analysis [2,3]. Therefore, we can further understand the structural features and dynamics mechanism of complex systems by studying the basic topological properties of networks. Many algorithms have been proposed to construct different complex networks from time series [7], such as visibility graphs [8,9], space state networks [10], recurrence networks [2,3,11], and nearest-neighbor networks [12,13].

Recurrence is a basic characteristic of many complex dynamical systems, which can be used to describe the

dynamics behavior of systems. Eckmann *et al.* [14] developed the method of recurrence plots (RPs) to visualize the recurrence property of complex dynamical systems. A remarkable advantage of this method is that it is very suitable for short and even nonstationary time series. Applications of the method of RPs can be found in various fields of research such as physiology, neuroscience, earth sciences, engineering, biology, and finances. In order to quantify the structures of the recurrence plots, Zbilut and Webber developed the recurrence quantification analysis (RQA) based on linear and diagonal line structures of recurrence plots [15,16]. Most of these measures of complexity are available on the TOCSY software platform [17]. Cross recurrence plot [18,19] and joint recurrence plot [20] are bivariate and multivariate extensions of the RPs, respectively.

Recently, Donner *et al.* [2,3] and Marwan *et al.* [11] proposed the recurrence network based on the method of RPs. This idea can be considered as a complementary view on the RQA, allowing us to gain additional information from corresponding network-theoretic measures which cannot be obtained by RQA. They considered the phase-space state vectors $X(i)$ (defined in Sec. II) as nodes of a complex network and identify the recurrence matrix of the original time series with the adjacency matrix of an associated complex network. In this way, an undirected and unweighted network is represented by a binary adjacency matrix A_{NN} (defined in Sec. II). Recurrence networks have been used to investigate many model systems such as logistic map, Hénon map, Lorenz system, Rössler system, and Bernoulli map [3,11,21], and real economic series [22].

---
*Corresponding author: yuzg1970@yahoo.com

It is well known that fractional Brownian motion (FBM) described by the Hurst index H ($0 < H < 1$) is a self-similar process with stationary increments [23]. The FBM with $H = 1/2$ is in fact the classical Brownian motion. The correlation between increments of the FBM is negative if $0 < H < 1/2$ and positive if $1/2 < H < 1$. The sample paths of FBM series are relatively more rough and variable for small Hurst index H, while the sample paths of FBM series are more smooth for large Hurst index H.

In this work, we try to reveal the relationship between FBM and its related recurrence network from the perspective of network structure. This prompted us to further study the fundamental topological and fractal properties of recurrence networks constructed from FBMs. We think that applying recurrence network analysis (RNA) to FBM can yield results which are theoretically meaningful. The reasons are as follows. (a) Visibility graphs and recurrence networks are two main classes of methods to map time series to networks. Recently, some works have been done to study the relationship between the exponents of newly developed methods (including visibility graphs) and the Hurst index of the associated FBMs [24–26]. (b) Donges *et al.* [21] have proposed an analytical framework for RNA of time series of chaotic maps and stochastic processes (such as uniformly distributed noise and Gaussian noise). FBMs are generalizations of Gaussian noise. (c) Donner *et al.* [22] applied RNA to study the real economic time series. And it is well known that FBM has been used as a theoretical framework to study economic time series [23]. In 1999, Riley *et al.* [27] applied the RQA technique for analyzing center of pressure (COP) signals and the nonstationarity of the COP is expected from a consideration of COP trajectories as FBM.

The remainder of this paper is organized as follows. In Sec. II, we adopt the recurrence plot method to construct recurrence networks. In Sec. III, we investigate the basic topological characteristics of the recurrence networks constructed from FBMs. We next introduce the random sequential box-covering method [28] to calculate the fractal dimension of the recurrence networks in Sec. IV. In Sec. V, we introduce an improved algorithm developed by our group [29], which is based on the modified fixed-size box-counting algorithm [30], to probe the multifractal behavior of recurrence networks. We finally draw some conclusions in Sec. VI.

II. RECURRENCE NETWORK

The method of recurrence plots is based on the theory of phase-space reconstruction introduced by Packard *et al.* [31]. In order to easily construct a more suitable space and then to reveal more meaningful information from original time series, Packard *et al.* [31] proposed the derivative reconstruction method and time delay method to reconstruct a finite-dimensional phase space. However, in practice, we do not know any prior information of time series; therefore, the latter method is widely used to reconstruct phase space of time series. For a given scalar time series $\{x_i, i = 1, 2, \ldots, L\}$, we construct the delay vectors

$$X(i) = (x_i, x_{i+\tau}, \ldots, x_{i+(m-1)\tau}), \quad X(i) \in \mathbb{R}^m, \quad (1)$$

for $i = 1, 2, \ldots, N$, where $N = L - (m - 1)\tau$, m is the embedding dimension, and τ is the time delay. Takens' embedding theorem ensures that we can recreate a topologically equivalent m-dimensional phase space from an infinite noise-free time series data by means of the time delay method [32]. The most significant advantage of phase-space reconstruction is that it can preserve the geometrical invariants of the original system, such as the fractal dimension and the Lyapunov exponents [32]. So we can investigate much about the dynamics characteristics of time series in phase space more easily. The basic embedding theorem of phase-space reconstruction assumes that we can choose the delay time τ without any limitation and the embedding dimension m under the condition of $m \geqslant 2d + 1$, where d is the fractal dimension of the underlying attractor. However, since the observed time series data sets are finite and noisy in the most common case, the selection of the time delay τ and the embedding dimension m is rather important for the quality of the phase-space reconstruction.

The binary recurrence matrix $R_{NN} = (R_{i,j})_{NN}$ is defined as

$$R_{i,j} = \Theta(\varepsilon - \|X(i) - X(j)\|), \quad i, j = 1, 2, \ldots, N, \quad (2)$$

where ε is a threshold distance, $\|\cdot\|$ is a suitable norm (e.g., the L_1 norm, the Euclidean norm, and the L_∞ norm) in the considered phase space and $\Theta(x)$ is the Heaviside step function [i.e., $\Theta(x) = 0$ if $x < 0$, and $\Theta(x) = 1$ otherwise]. The resulting matrix R_{NN} is a symmetric matrix where the elements $R_{i,j} = 0$ or 1. Moreover, the matrix R_{NN} exhibits the line of identity (the main diagonal) $R_{i,i} = 1$. In a two-dimensional space, the recurrence plot is described by using different colors for different values of the recurrence matrix, e.g., plotting a black dot at the coordinates (i, j) if $R_{i,j} = 1$, and a white dot if $R_{i,j} = 0$. Thus the recurrence plot always has a black main diagonal line.

Now we obtain the adjacency matrix $A_{NN} = (A_{i,j})_{NN}$ of the recurrence network from the recurrence matrix R_{NN} as

$$A_{i,j} = R_{i,j} - \delta_{i,j}, \quad (3)$$

where $\delta_{i,j}$ is the Kronecker δ function introduced here in order to avoid self-loops [3]. In a complex network, each state vector $X(i)$ of the reconstructed phase space represents a single node. The topological structure of the recurrence network can be described with the adjacency matrix A_{NN}, and the elements $A_{i,j} = 1$ and $A_{i,j} = 0$ correspond to connection and disconnection, respectively. And the size of the network is N.

As mentioned above, the choice of the time delay τ and the embedding dimension m plays an important role in the recurrence plot method. If the time delay τ selected is too small, each coordinate of the vector $X(i)$ will be so close to each other that the trajectories of the reconstructed phase space are compressed along the identity line, and this phenomenon is referred to as redundance. If the time delay τ selected is too large, the coordinates of the vector $X(i)$ are completely independent of each other and then the reconstructed attractor dynamics become causally disconnected, and this phenomenon is referred to as irrelevance [33]. At present, autocorrelation function [34] and mutual information method [35] are the most common approaches for the estimation of the time delay τ. Fraser *et al.* [35] proposed a recursive method of calculating mutual information and pointed out that the first local minimum of

mutual information is the best criterion for choosing time delay τ in phase-space reconstruction from time series data.

Takens' embedding theorem gives us a way to estimate the embedding dimension m. This is to say that all self-intersections of the orbit (which is the reconstructed attractor) in the reconstructed phase space will be eliminated for any embedding dimension $m \geqslant 2d + 1$. The attractor will be completely unfolded in this embedding dimension m. But, in practice, since the dimension d is unknown in many cases, we cannot directly calculate the embedding dimension m from the Takens' embedding theorem. Many algorithms based on computing some invariants on the attractor have been proposed to calculate the minimum embedding dimension m. The most popular method for calculating the minimum embedding dimension is the False nearest-neighbors (FNN) algorithm [36,37]. According to the Takens' embedding theorem, we assume that m is qualified as an embedding dimension. If any two points are close to each other in the m-dimensional phase space, then they are still close to each other in the $(m + 1)$-dimensional phase space. We call these two points true neighbors; otherwise, they are false neighboring points. The main idea of the FNN algorithm is to measure the percentage of false nearest neighbors along a signal trajectory change with increasing embedding dimension. The optimal embedding dimension means that there are no false neighbors and self-intersections in the phase space. This indicates that the minimum embedding dimension is that for which the percentage of false nearest neighbors drops to zero or nearly zero for a given tolerance level for the first time [36].

The threshold distance ε is another key parameter of an RP. The selection of the threshold ε depends strongly on the system considered. If ε is too small, there may be almost no recurrence points and we cannot learn anything about the recurrence structure of the underlying system. On the other hand, if ε is too large, almost every point is a neighbor of every other point, which leads to a lot of artifacts and redundant information [38]. Therefore, special attention has been required of its choice. In practice, the most common method is to set ε for a certain proportion of the standard deviation σ of the original time series. However, Riley and Van Orden suggested choosing ε such that the recurrence point density remains low (often smaller than 5%) [39]. This method is often used in RQA. The advantage of choosing an adaptive recurrence threshold by using a fixed recurrence rate in RQA is that it can preserve the recurrence point density and then allows us to compare the results of recurrence quantification analysis of different systems. It is easy to imagine that there is no direct relationship between recurrence rate or link density and network connectivity. And it is so difficult for us to find a fixed recurrence rate which all recurrence networks obtained at recurrence threshold ε calculated from the fixed recurrence rate are connected. However, we restrict our attention to the consideration of a connected network in this article. Therefore, we do not adopt the fixed recurrence rate for obtaining such an appropriate recurrence threshold. If we do so, then we will not be able to study the topological and fractal properties of the entire network. In other words, we can only focus on the disconnected components or the largest connected component of each recurrence network.
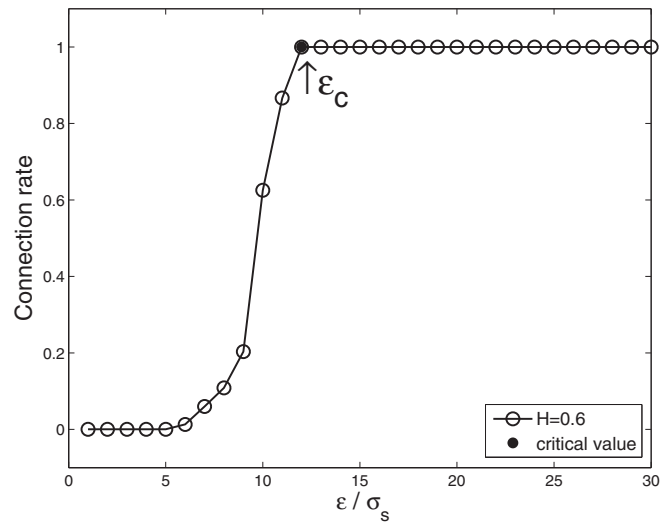

FIG. 1. Relationship between the recurrence threshold ε and the connection rate of the recurrence network constructed from fractional Brownian motion series of length $L = 2^{12}$ with Hurst index $H = 0.6$.

The critical phenomenon is one of the most interesting findings of complex networks. In 1959, Erdős *et al.* [40] introduced the classical random-graph model and studied the structural phase transition of the birth of the giant connected component in the network architectures. Every pair of nodes of random graph is connected with probability p. They found that there exists a critical probability p_c where a giant connected component was formed and it can be spread across the entire network. If the probability p is less than this critical probability p_c, the network is composed of disconnected components. Similar to the critical behavior of random-graph theory, we study the critical connectivity of the recurrence networks by examining the size of the largest connected component and then determine the critical recurrence threshold ε_c. Here we first employ the connection rate of the network to quantify the connectivity of the recurrence network, which is defined as the number of nodes of the largest connected component divided by the size of the network. Secondly, we observe the change of connection rate of the network with the increase of the parameter ε. It can be easily imagined that the connection rate of the network increases when the parameter ε becomes larger, as illustrated in Fig. 1. In Fig. 1, we set the recurrence threshold ε ranging from 0.01σ to 0.3σ with a step of $\sigma_s = 0.01\sigma$, where σ is the standard deviation of the original FBM series. Finally, we choose an appropriate recurrence threshold ε_c which is the minimal value of ε such that the connection rate of the network reaching to 1. As can be seen in Fig. 1, we set the critical recurrence threshold $\varepsilon_c = 0.12\sigma$. The recurrence network obtained at recurrence threshold ε_c will be connected. The threshold ε beyond this critical value ε_c will result in redundant connections among nodes, and threshold ε below this critical value ε_c will lead to a number of disconnected components where each component only contains a connected subnetwork. Consequently, we select this suitable recurrence threshold ε_c to construct the recurrence network and then investigate its topological and fractal properties. In addition, we also notice that the critical recurrence threshold ε_c decreases with the increase of the Hurst index H from 0.4 to 0.95. We know that the FBM

series is relatively more smooth and regular for large Hurst index H. The consequence is that there are many data points in the original FBM series mapped to state vectors which are close to each other in a dense region of the phase space so that the largest connected component of the recurrence network contains more nodes than the one of the network with the small Hurst index H. The specific explanation for this phenomenon can be found in the second subsection of the Sec. III.

In this work, we consider FBM of length $L = 2^{12}$ with different Hurst indices H ranging from 0.05 to 0.95 (the step difference is 0.05). Recurrence networks can be constructed by the following steps.

(i) For a given FBM time series, we use the mutual information method [35,41] and the FNN algorithm [36] to calculate the time delay τ and the embedding dimension m, respectively. These two procedures are available on the TOCSY software platform [17]. The values of embedding dimensions m we obtained vary from 5 to 7, and those of the time delay τ vary from 10 to 20.

(ii) We use the connection rate of the recurrence network to determine the suitable threshold distance ε_c [42]. We observe the connection rate of the network reaching 1 when the parameter ε ranges from 0.01σ to 0.8σ with a step of $\sigma_s = 0.01\sigma$, where σ is the standard deviation of the original FBM series. The connection rate of the network can be calculated by Matlab-BGL toolbox [43] in Matlab.

(iii) Based on the above steps, we can calculate the recurrence matrix R_{NN} by Eq. (2). Then we obtain the binary adjacency matrix A_{NN} of an unweighted and undirected recurrence network by Eq. (3). As a result, the recurrence network is also connected.

For clarity of visualization, we here only draw the recurrence network for the FBM series of length $L = 2^8$ with Hurst index $H = 0.6$. After obtaining the adjacency matrix A_{NN} of recurrence network according to the above three steps, we convert the adjacency matrix A_{NN} into "Pajek" [44] format and then we adopt the Pajek, which is a freely available software platform for visualizing and analyzing complex networks to visualize the recurrence network. As can be clearly seen in
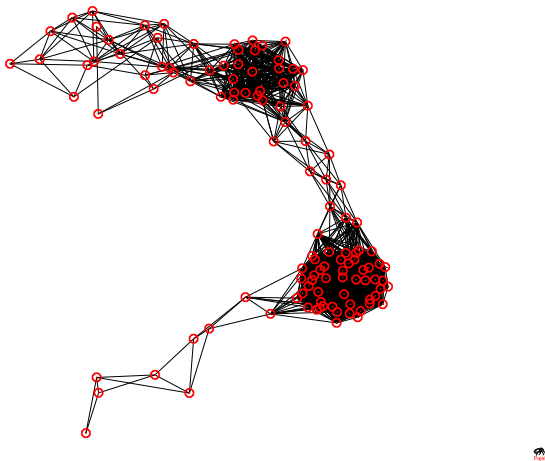

FIG. 2. (Color online) Recurrence network constructed from fractional Brownian motion series of length $L = 2^8$ with Hurst index $H = 0.6$.

Fig. 2, the recurrence network constructed from the associated FBM series is connected.

In addition, we find that the connection rates of recurrence networks constructed from FBMs with Hurst indices $H = 0.05, 0.1, \ldots, 0.3$, and 0.35 are far less than 1. In these cases, the recurrence networks are not connected. So, in the following sections, we only consider connected networks with Hurst indices H from 0.4 to 0.95.

III. FUNDAMENTAL TOPOLOGICAL PROPERTIES

In this section, we numerically study the basic topological features of recurrence networks including the degree distribution, the clustering coefficient and the motif distribution. Recent works have shown that a large number of real-world networks are referred to as scale-free networks because the degree distribution $P(k)$ follows a power law

$$P(k) \sim k^{-\alpha}, \tag{4}$$

with the degree exponent α varying in the range $2 < \alpha < 3$ [5,6,45]. The degree distributions of the visibility graphs constructed from FBMs have power-law tails [8,24,46]. In addition, Xie *et al.* [25] found that horizontal visibility graphs constructed from FBMs have exponential degree distributions

$$P(k) \sim e^{-\lambda k}, \tag{5}$$

and the degree exponent λ increases with Hurst index H.

It has been shown that many real-world complex networks share similar universal statistical features, such as the small-world character and the scale-free distribution, but may demonstrate different local structure characteristics [4,5,47]. An in-depth study of motif distribution can help us to understand the design principles of complex networks on the local structure level [47,48]. In 2004, Milo *et al.* [48] developed an approach for comparing network local structures, basing on the significance profile. They calculated the triad significance profile for networks from different fields and found that networks with similar characteristic profiles are grouped into superfamilies.

A. Degree distribution

Degree distribution is one of the most fundamental and important topological properties of complex networks. We simulated FBMs with different Hurst indices H ranging from 0.40 to 0.95 with an increment of 0.05. For each value of H, we generated 1000 realizations and then calculated the average degree distribution. For example, we give the average degree distribution of recurrence networks constructed from FBMs with Hurst index $H = 0.6$ in Fig. 3. We find that all the recurrence networks constructed from FBM series exhibit exponential degree distributions. We estimated the degree exponents λ and display the average degree exponents $\langle \lambda \rangle$ in Fig. 4. From Fig. 4, we can see that the parameter λ increases first and then decreases with the increase of H. The inflection point is at around $H = 0.8$. We find that the relationship between H and $\langle \lambda \rangle$ can be fitted by a cubic polynomial function which is also shown in Fig. 4.
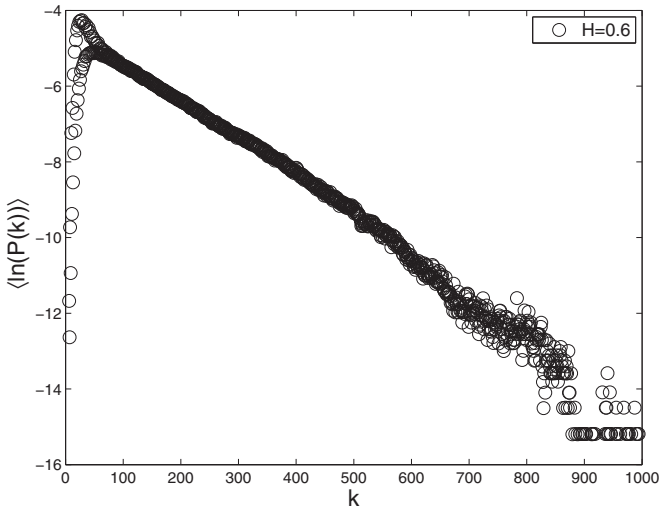
FIG. 3. Degree distribution of one recurrence network constructed from fractional Brownian motion with Hurst index $H = 0.6$.

B. Clustering coefficient

The clustering coefficient measures the density of triangles in a complex network. The definition of the clustering coefficient given by Watts and Strogatz in Ref. [4] has been used quite widely in complex network. The local clustering coefficient C_i is defined as

$$C_i = \frac{2E_i}{k_i(k_i-1)} = \frac{\sum_{j,h} A_{i,j} A_{j,h} A_{h,i}}{k_i(k_i-1)}, \qquad (6)$$

where k_i is the degree of node i, E_i is the actual number of edges among k_i nearest-neighbor nodes of the node i. The clustering coefficient of the whole network is then given by the average of C_i over all the nodes in the entire network:

$$C = \frac{1}{N} \sum_i C_i. \qquad (7)$$
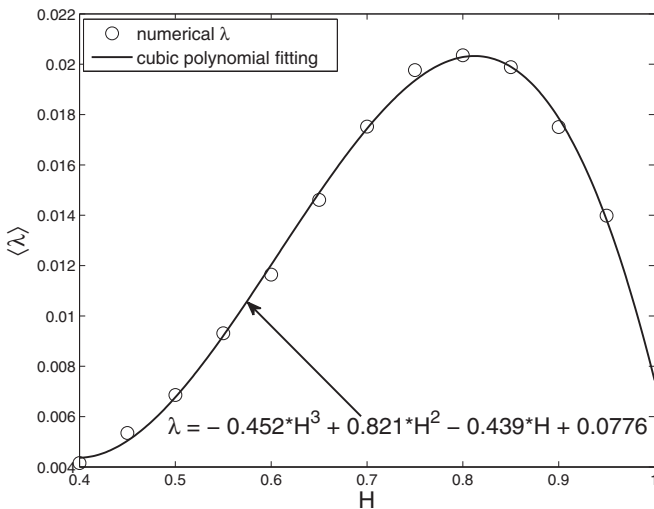
FIG. 5. All two triples centered on vertex i.

From the geometrical point of view, the local clustering coefficient C_i also can be defined as

$$C_i = \frac{\text{number of triangles connected to vertex } i}{\text{number of triples centered on vertex } i}, \qquad (8)$$

where a triple represents a vertex with edges connected to any two neighbor vertices. There are two different triples as shown in Fig. 5. The triple T_1 will occur if the three vertices are all close to each other. Conversely, the triple T_2 will occur if the vertex i is connected to its two neighbor vertices j and k, but vertices j and k are not connected. In network topology, the triangle structure T_1 means transitivity and stability in the network.

In this paper, we study the dependence of the clustering coefficient C of the recurrence networks against the Hurst index H of the original FBMs. For each H, we simulated the FBM 1000 times; hence we obtained 1000 FBM series. For each FBM series, a recurrence network was constructed and its clustering coefficient C was calculated. We display the relationship between H and the average clustering coefficient $\langle C \rangle$ of recurrence networks in Fig. 6. From Fig. 6, we can see that the average clustering coefficient $\langle C \rangle$ increases with the Hurst index H. The results show that there are more triangle structures in the recurrence network when the Hurst index H increases from 0.4 to 0.95. This means that the transitive and stable structure is more common for large Hurst indices. This phenomenon can be easily explained by the following points. It is well known that the Hurst index characterizes the raggedness and irregularity of FBM. As already mentioned, the FBM is a

FIG. 4. Relationship between H of fractional Brownian motion and average degree exponent $\langle \lambda \rangle$ of the associated recurrence networks. Here the average is calculated from 1000 realizations.
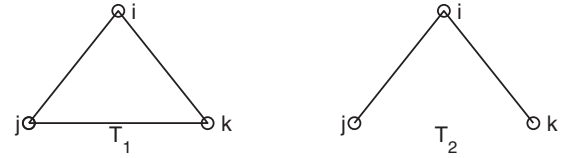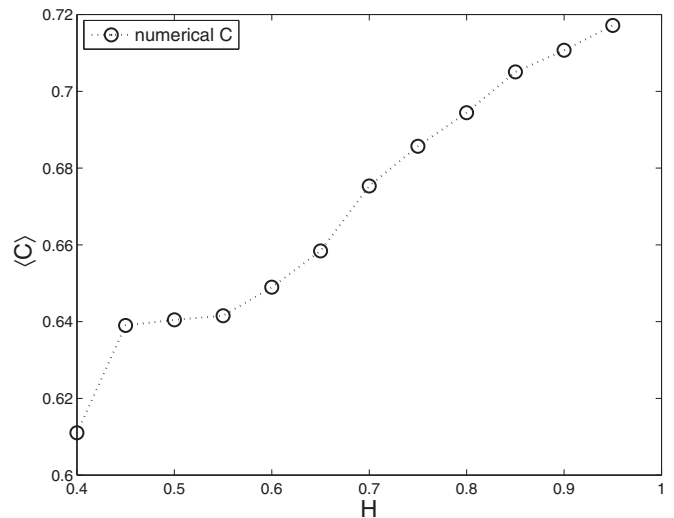

FIG. 6. Relationship between H of fractional Brownian motion and average clustering coefficient $\langle C \rangle$ of the associated recurrence networks. Here the average is calculated from 1000 realizations.

self-similar process with stationary increments and possesses long-range dependence. The Hurst index H $(0 < H < 1)$ is a measure of the intensity of long-range dependence in a FBM series. More specifically, the FBM with $H = 0.5$ indicates the absence of long-range dependence. And the closer Hurst index H is to 1, the greater the extent of long-range dependence or persistence. The Hurst index H less than 0.5 corresponds to antipersistence, which means that the process displays strong negative correlation and fluctuates violently. For large Hurst index H, the FBM series is relatively more smooth and regular. The result is that close data points in the original FBM series are mapped to state vectors $X(i)$ which are close to each other in a dense region of the phase space so that these nodes $X(i)$ are more likely to be connected to each other in recurrence network. As expected, there are many more transitive and stable structures T_1 to appear in the recurrence network constructed from the FBM series with large Hurst index H. However, the FBM series with small Hurst index H is relatively more rough and irregular. As a consequence of this, these close points in the original FBM series are mapped to state vectors $X(i)$ in a sparse region of the phase space that are less likely to be mutually connected, and therefore the triple T_2 will be more common. From this point of view, the recurrence network reflects the smoothness and regularity of the FBMs to some extent.

C. Motif distribution

Because it is very time consuming to study next a few properties of large complex networks, we only generated 100 realizations of FBM for each value of Hurst index H and calculated the average in the following.

Research has shown that subgraphs or motifs are the building blocks of complex networks and the superfamilies of networks can be defined as the network motif patterns of occurrence [47,48]. Distinct from the degree distribution and the clustering coefficient, the occurrence frequency of small subgraphs or motifs can characterize the local structural properties of real-world networks and then map the relation between the function and the local structure of real-world systems [47]. Xu *et al.* [12] observed the superfamily phenomenon in the nearest-neighbor networks constructed from different time series. They also found that the distribution of network motif ranks can be used to distinguish and to characterize different types of dynamics in periodic, chaotic, and periodic with noise processes [12]. Xie *et al.* [25] calculated the frequencies of occurrence of the six motifs of size four within the horizontal visibility graphs constructed from FBMs.

In this work, the constructed recurrence networks are connected and undirected, so here we only consider motifs with four nodes as in Ref. [25]. Figure 7 shows all six different
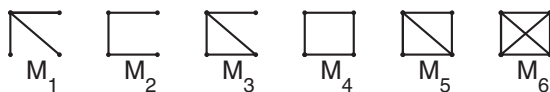
network motifs of size four in connected and undirected networks. These motifs reflect the different local structure characteristics in network. There are two extreme blocks: motif M_1 and motif M_6. The motif M_1 means the most irregular and nontransitive structure that will appear if the node is connected to its three neighbor nodes, but these neighbors are not connected to each other. On the contrary, the motif M_6 indicates the most transitive structure that will appear if the three neighbors are also connected to each other. The relative occurrence frequencies of motifs [25] are defined as

$$P(M) = \frac{n(M)}{\sum_{M=M_1,\dots,M_6} n(M)}, \qquad (9)$$

where $n(M)$ is the number of motif M in the network. After constructing the recurrence networks based on the recurrence plot method described above, we calculated the occurrence frequencies of various motifs within the recurrence networks by the network motif detection tool provided by Milo *et al.* [49]. For each Hurst index H, which runs from 0.40 to 0.95 with a step of 0.05, 100 realizations of FBMs were generated. Then we constructed these time series into 100 recurrence networks and obtained the average of $P(M)$.

In Fig. 8, we rearrange the relative occurrence frequencies $\langle P(M) \rangle$ in descending order for different Hurst indices H. As we can see from Fig. 8, these seemingly unrelated recurrence networks are divided into two superfamilies based on the very similar motif rank distributions. Figure 8(a) shows a superfamily determined by the motif rank $M_2 M_3 M_1 M_5 M_6 M_4$, which includes the recurrence networks constructed from FBMs with Hurst indices $H = 0.4, 0.45, 0.5, 0.55,$ and 0.6. The rest of the recurrence networks with Hurst indices $H = 0.65, \dots, 0.95$ belong to another superfamily and the motif rank pattern is $M_2 M_3 M_5 M_6 M_1 M_4$ [Fig. 8(b)]. In addition, three particular motifs M_1, M_5, and M_6 play an important role
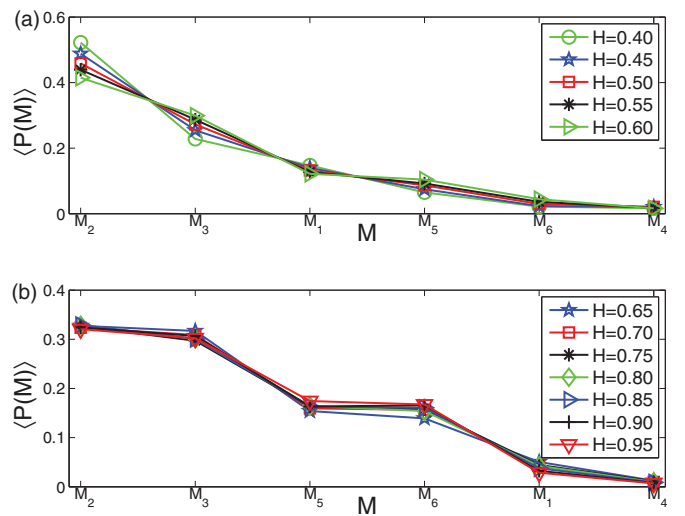

FIG. 8. (Color online) Network motif rank distributions of FBMs with different Hurst indices H. (a) Motif rank pattern $M_2 M_3 M_1 M_5 M_6 M_4$ for $0.4 \leqslant H \leqslant 0.6$. (b) Motif rank pattern $M_2 M_3 M_5 M_6 M_1 M_4$ for $0.65 \leqslant H \leqslant 0.95$. Here the average is calculated from 100 realizations.
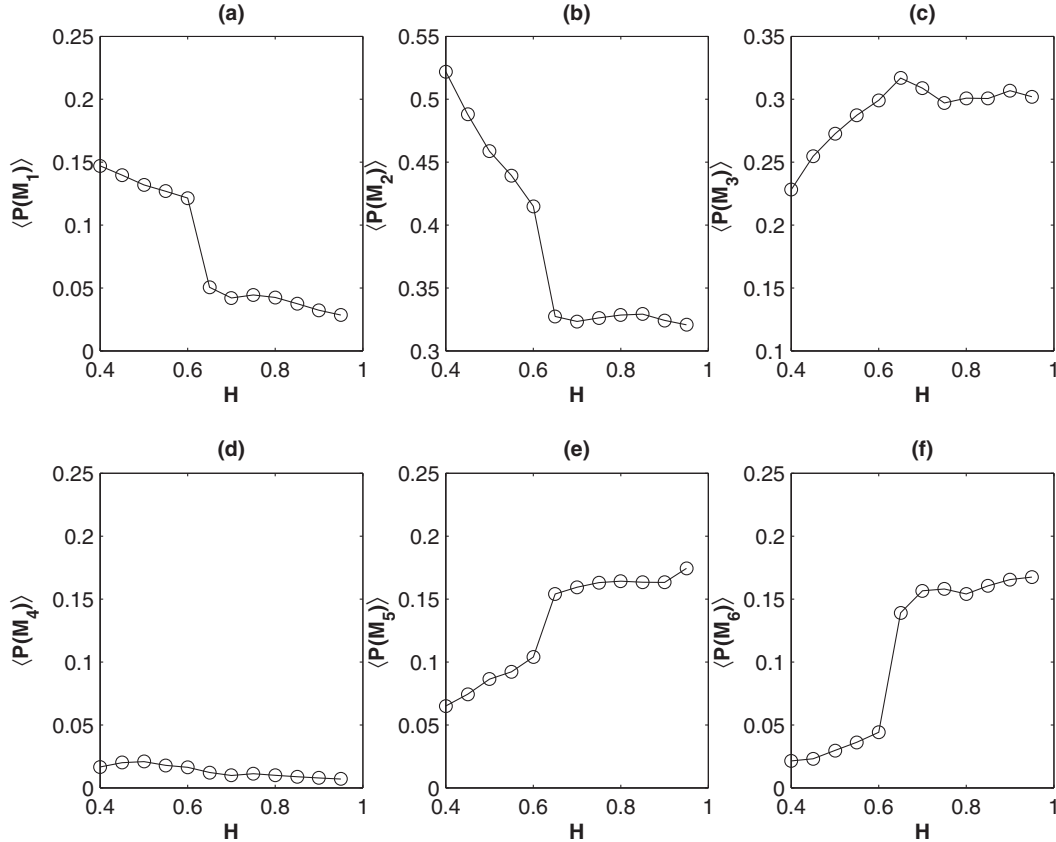

FIG. 7. All six network motifs of size 4 in connected and undirected network. These motifs are labeled M_1, M_2, M_3, M_4, M_5, and M_6, respectively.

FIG. 9. Dependence of average occurrence frequencies of motifs M_1, M_2, M_3, M_4, M_5, and M_6 on the Hurst indices H. Here the average is calculated from 100 realizations.

in the classification of recurrence networks we constructed because their order determines the motif rank distributions. A similar phenomenon was also observed in Refs. [12,13]. They gave a detailed explanation for this common phenomenon. Figure 9 further illustrates the dependence of $\langle P(M) \rangle$ with respect to the Hurst index H. More specifically, the occurrence frequency $\langle P(M_1) \rangle$ of motif M_1 strictly monotonically decreases with the increase of the Hurst index H [see Fig. 9(a)]. In contrast to the motif M_1, the frequencies $\langle P(M_5) \rangle$ and $\langle P(M_6) \rangle$ increase with the increase of the Hurst index H [see Fig. 9(e) and Fig. 9(f)]. We also note that the fluctuation of the frequencies $\langle P(M_4) \rangle$ is comparatively small in Fig. 9(d), which means that the motif M_4 almost does not appear in all of the recurrence networks. These results indicate that there are more regular and transitive structures in the networks when the Hurst index H varies from 0.4 to 0.95. That is to say, the fully transitive motif M_6 will be common in these recurrence networks constructed from the FBM series with large Hurst index H than the ones with small Hurst index H. On the contrary, the irregular and nontransitive structure such as M_1 will be more common for these network with small Hurst index H. These trends roughly coincide with the ones in the previous subsection. It should be noted that two triples T_1 and T_2 in Fig. 5 are just two motifs with three nodes in an undirected network. Measuring and analyzing the density distribution of the motifs with four nodes may be seen as a generalization of the aforementioned transitivity concept. Therefore, as mentioned in the previous subsection, we can

give a similar explanation for these trends in this subsection. In this sense, recurrence networks capture the correlation of the associated FBMs.

IV. FRACTAL DIMENSION

In 1967, Mandelbrot introduced the fractal idea in Ref. [50]. In fractal geometry, a fractal object is self-similar because it contains small parts similar to the whole [51,52]. Recently, the fractal and self-similarity properties of complex networks have been studied extensively in various fields and systems [30,53,54]. Song *et al.* [55] found that many real-world networks such as the worldwide web (WWW), social networks, protein-protein interaction (PPI) networks, and cellular networks consist of self-repeating patterns. They also believed that these complex networks are self-similar under a certain length scale. After the small-world character and scale-free property, self-similarity has become the third basic characteristic of complex networks.

To gain further understanding of complex networks, numerous algorithms have been developed to calculate the fractal dimension of complex networks. Song *et al.* [56] proposed to calculate the fractal dimension via a box-counting method. Kim *et al.* [28,54] investigated the skeleton and fractal scaling in complex networks using an improvement algorithm which is a modified version of the original method introduced by Song *et al.* Then Zhou *et al.* [57] developed an alternative algorithm, based on the edge-covering box counting, to detect

self-similarity of cellular networks. In this section, we adopt the random sequential box-covering method proposed by Kim *et al.* [28] for calculating the fractal dimensions of recurrence networks.

For a given network, let $N_B(l_B)$ be the smallest number of boxes of lateral size l_B which are needed to cover the entire network. The fractal scaling implies the power law relationship between $N_B(l_B)$ and l_B; the fractal dimension d_B is then given by

$$N_B(l_B) \sim l_B^{-d_B}. \tag{10}$$

Usually, the fractal dimension d_B can be obtained by fitting the linear relationship between $N_B(l_B)$ and l_B in a log-log plot.

Before introducing the random sequential box-covering algorithm [28], we use Floyd's algorithm [58] of Matlab-BGL toolbox [43] to calculate the shortest-path distance matrix D for each network according to the adjacency matrix A_{NN} of the recurrence network. The random sequential box-covering algorithm [28] can be described as follows. We start with all vertices labeled as not burned.

(i) Then select a vertex randomly at each step; this vertex serves as a seed and then consider the seed as the center of a box.

(ii) For the center of the box, search all the neighbor vertices within distance l_B and burn all vertices which are found but have not been burned yet. Assign the newly burned vertices to the new box. If no newly burned vertex is found, then discard this box.

(iii) Repeat steps (i) and (ii) until all vertices in the entire network are assigned to their respective boxes.

In this work, we simulated FBM series with different Hurst indices H ranging from 0.4 to 0.95 in the step of 0.05. For each H, we simulated 100 FBM time series and then constructed the obtained series into 100 recurrence networks. Apparent power law behaviors of the two typical empirical recurrence networks constructed from FBM series with different Hurst indices are shown in Fig. 10. The fractal dimension d_B is the absolute
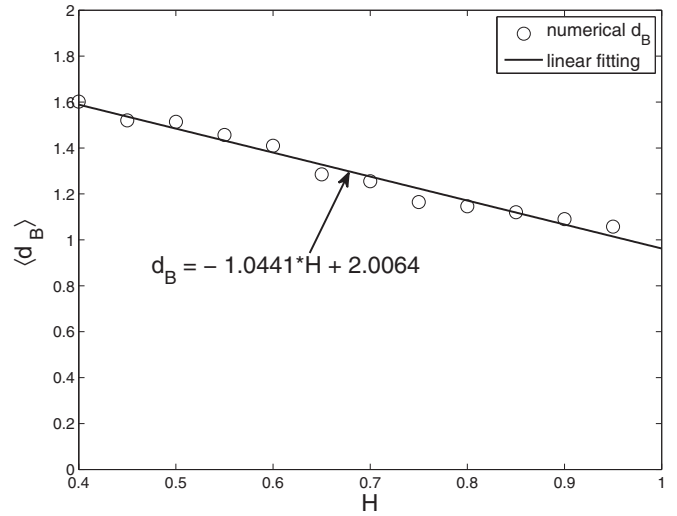
FIG. 11. Relationship between H of fractional Brownian motion and average fractal dimension $\langle d_B \rangle$ of the associated recurrence networks. Here the average is calculated from 100 realizations.

value of the slope of linear regression between $\ln N_B(l_B)$ and $\ln l_B$ for each Hurst index. Figure 11 shows the relationship between Hurst index H and the average fractal dimension $\langle d_B \rangle$ over 100 realizations. As we can see from Fig. 11, the average fractal dimension $\langle d_B \rangle$ decreases with increasing H. Furthermore, it is surprising that the curve shows a nice linear relationship:

$$\langle d_B \rangle = 2.0064 - 1.0441H, \tag{11}$$

which approximates the theoretical relationship between Hurst index H and the fractal dimension d of the graph of FBM $d = 2 - H$. Our numerical results show that the fractal dimension of the recurrence networks constructed is very close to that of the graph of the original FBMs. In other words, the fractality of FBMs is inherited in their recurrence networks. We can explain here why the two fractal dimensions are so closely related that the Hurst index H of the FBM series can be approximately estimated from the perspective of the complex network. As it has already been mentioned, the pairs of nodes in the recurrence network can be connected only when the two corresponding state vectors $X(i)$ in phase space are close enough so that the phase-space distance between them is less than the critical recurrence threshold ε_c. This is to say that recurrence networks we constructed are random geometric graphs faithfully representing the geometry of a set in phase space. Hence neighborhood sizes around a node in the network as well as around the corresponding state vector in phase space will show the same scaling behavior. This results in analogous behavior of the derived fractal dimensions.

So far, we have numerically studied the basic topological properties and the fractal dimensions of the recurrence network. More recently, some chaotic model systems such as the logistic map, Hénon map, generalized baker's map, and Bernoulli map, and periodic and two-dimensional quasiperiodic motions have been studied analytically by Donner *et al.* [59] and Donges *et al.* [21] from the point of view of the ε-recurrence network. To better understand the interrelationships
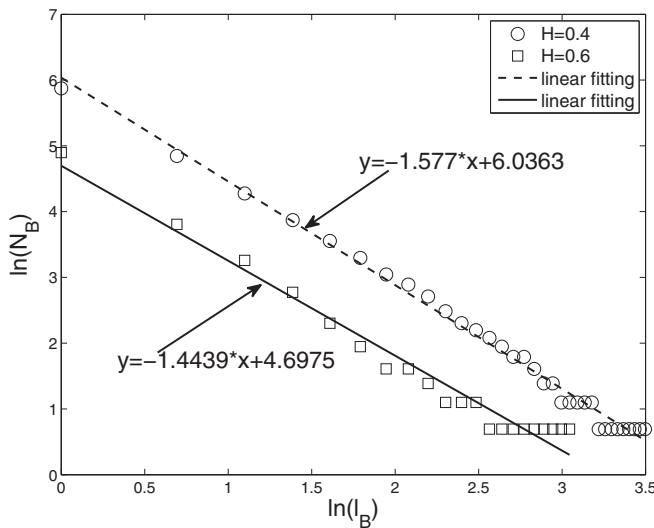

FIG. 10. Fractal scaling of recurrence networks constructed from FBMs with Hurst indices $H = 0.4$ and 0.6. The fractal dimension is the absolute value of the slope of the linear fit.

between network properties and dynamical system, they defined some continuous measures based on well-known graph theoretical measures and gave two notions of dimension in phase space (clustering dimension and transitivity dimension). They have put forward a theoretical framework for these measures. Their results indicated that ε-recurrence networks show a strong relation between dynamical systems and graph theory [21,59]. Their work provides us with a possible way to derive the analytical results of these topological properties and dimensions for the recurrence network of FBM series in our future work.

V. MULTIFRACTAL ANALYSIS

In real world, two fractal objects may have the same fractal dimension but look completely different. For these real-world fractals, however, the tool of multifractal analysis shows better performance and seems more powerful than fractal analysis. Multifractal analysis has been successfully applied in a variety of fields such as financial modeling [60,61], biological systems (e.g. [62–65]), and geophysical data analysis (e.g. [66,67]). Wang *et al.* [30] applied the modified fixed-size box-counting algorithm to explore the multifractal behavior of some theoretical networks, namely scale-free networks, small-world networks, random networks, and a kind of real networks, namely PPI networks of different species. Their numerical results indicate that multifractality exists in scale-free networks and PPI networks, while for small-world networks and random networks their multifractality is not clear-cut.

Fixed-size box-covering algorithm [68] is one of the most common and important methods of multifractal analysis. For a given measure μ with support set E in a metric space, we consider the partition sum

$$Z_\epsilon(q) = \sum_{\mu(B) \neq 0} [\mu(B)]^q, \tag{12}$$

where $q \in \mathbb{R}$ and the sum runs over all different nonempty boxes B of a given size ϵ in a covering of the support set E. From the definition above, we can obtain $Z_\epsilon(q) \geqslant 0$ and $Z_\epsilon(0) = 1$. The exponent $\tau_1(q)$ of the measure μ can be defined as

$$\tau_1(q) = \lim_{\epsilon \to 0} \frac{\ln Z_\epsilon(q)}{\ln \epsilon}, \tag{13}$$

and the generalized fractal dimensions of the measure μ are defined as

$$D(q) = \frac{\tau_1(q)}{q - 1}, \tag{14}$$

for $q \neq 1$, and

$$D(q) = \lim_{\epsilon \to 0} \frac{Z_{1,\epsilon}}{\ln \epsilon}, \tag{15}$$

for $q = 1$, where $Z_{1,\epsilon} = \sum_{\mu(B) \neq 0} \mu(B) \ln \mu(B)$. The linear regression of $[\ln Z_\epsilon(q)]/(q - 1)$ against $\ln \epsilon$ for $q \neq 1$ gives numerical estimates of the generalized fractal dimensions $D(q)$, and similarly a linear regression of $Z_{1,\epsilon}$ against $\ln \epsilon$ for $q = 1$. In particular, $D(0)$ is the box-counting dimension (or fractal dimension), $D(1)$ is the information dimension, and $D(2)$ is the correlation dimension. If the $\tau_1(q)$ or $D(q)$ curve

versus q is a straight line, the object is monofractal. However, if this curve is convex, the object is multifractal.

In order to calculate the exponents $\tau_1(q)$ and the generalized fractal dimensions $D(q)$ and then study the multifractality of networks, the measure μ of each box is usually defined as the ratio of the number of nodes covered by the box and the total number of nodes in the entire network. Wang *et al.* [30] proposed a modified fixed-size box-counting algorithm to calculate the $\tau_1(q)$ and $D(q)$ and then investigate the multifractal behavior of complex networks. Recently, Li *et al.* [29] made some improvements based on the modified fixed-size box-counting algorithm proposed by Wang *et al.* [30]. The improved algorithm [29] can be summarized as follows

(i) Initially, make sure all nodes in the entire network are not covered and no node is selected as a center of a box.

(ii) According to the size N of networks constructed, set $t = 1, 2, \ldots, 1000$ appropriately. Rearrange the nodes into 1000 different random orders. More specifically, in each random order, nodes which will be selected as a center of a box are randomly arrayed.

(iii) Set the radius r of the box which will be used to cover the nodes in the range $r \in [1, d]$, where d is the diameter of the network.

(iv) Treat the nodes in the tth random order that we got in (ii) as the center of a box, search all the neighbor nodes by distance r from the center, and cover all nodes which are found but have not been covered yet.

(v) If no newly covered nodes have been found, then discard this box.

(vi) Repeat steps (iv) and (v) until all the nodes are covered by the corresponding boxes. We denote the number of boxes in this box covering as $N(t, r)$.

(vii) Repeat steps (iv) to (vi) for all 1000 random orders to find a box covering with minimal number of boxes $N(t, r)$.

(viii) For the nonempty boxes B in the first box covering with minimal number of boxes $N(t, r)$, define the measure of this box as $\mu(B) = N_B / N$, where N_B is the number of nodes covered by the box B, and N is the size of the network. then calculate the partition sum $Z_r(q) = \sum_{\mu(B) \neq 0} [\mu(B)]^q$.
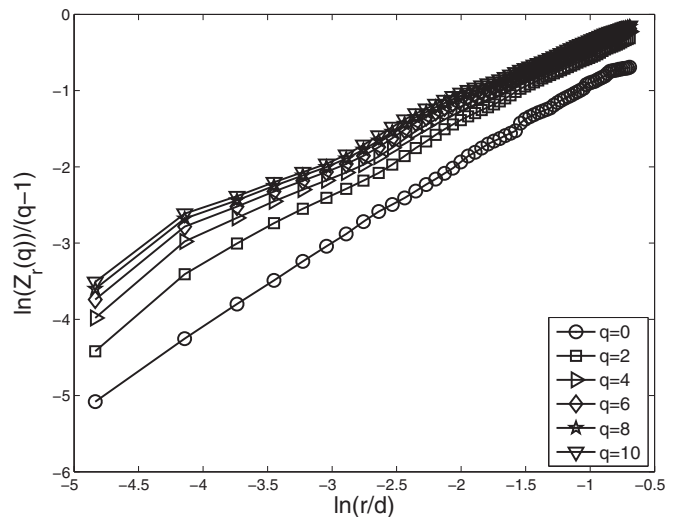

FIG. 12. Linear regressions for calculating the generalized dimensions of the recurrence network.

TABLE I. Comparison of recurrence networks transformed from FBM series with different Hurst indexes. Here the average is calculated from 100 realizations.

H	$\langle D(0) \rangle$	$\langle D(1) \rangle$	$\langle D(2) \rangle$	$\Delta D(q)$
0.40	1.632 955 359 4555 32	1.462 113 762 291 203	1.324 568 844 472 558	1.675 426 636 215 924
0.45	1.595 331 264 113 667	1.345 243 849 453 671	1.182 356 286 524 482	2.067 323 904 428 986
0.50	1.570 768 526 526 059	1.294 972 986 568 832	1.135 291 034 040 322	2.132 106 915 333 559
0.55	1.496 955 506 340 691	1.276 092 858 298 725	1.120 419 709 203 580	1.778 923 958 082 282
0.60	1.471 252 546 702 877	1.264 224 152 311 605	1.090 156 202 522 773	1.740 584 602 742 986
0.65	1.348 210 637 236 297	1.225 915 988 658 060	1.103 150 737 927 043	1.642 556 252 215 174
0.70	1.304 446 382 642 433	1.134 347 097 612 430	0.989 670 372 719 278	1.488 149 695 525 952
0.75	1.251 720 498 742 988	1.085 148 989 401 195	0.950 681 208 097 028	1.445 178 739 248 894
0.80	1.206 437 282 010 590	1.064 415 121 034 396	0.949 594 824 553 587	1.375 606 925 727 599
0.85	1.154 054 167 326 104	1.014 055 134 463 063	0.904 518 905 840 645	1.231 289 283 108 065
0.90	1.106 243 766 095 298	0.974 358 969 483 122	0.869 233 664 007 547	1.084 781 493 689 348
0.95	1.056 322 443 543 536	0.921 690 208 443 068	0.819 310 269 771 388	1.042 386 684 931 838

(ix) For different value of r, repeat steps (iii) to (viii) to calculate the partition sum $Z_r(q)$ and then use the $Z_r(q)$ for linear regression.

A key step of linear regression is to obtain the appropriate range of $r \in [r_{\min}, r_{\max}]$. Then we calculate the exponents $\tau_1(q)$ and generalized fractal dimensions $D(q)$ in the scaling ranges. In our calculation, we obtain the generalized fractal dimensions through a linear regression of $[\ln Z_r(q)]/(q-1)$ against $\ln(r/d)$ for $q \neq 1$, and similarly a linear regression of $Z_{1,r}$ against $\ln(r/d)$ for $q = 1$, where $Z_{1,r} = \sum_{\mu(B) \neq 0} \mu(B) \ln \mu(B)$.

Figure 12 shows the linear regression for the recurrence network constructed from FBM with Hurst index $H = 0.6$. The numerical results show that the best fit occurs in the range $r \in (2,10)$ for this case ($H = 0.6$). We select the best linear fit scaling range to calculate the exponents $\tau_1(q)$ and generalized fractal dimensions $D(q)$ and then to determine the multifractality of recurrence networks from the shape of these curves.

In this paper, we detect the multifractal behavior of recurrence networks using our improved version of the modified fixed-size box-counting algorithm introduced by Li *et al.* [29]. For each value of the Hurst index H, we averaged the results over 100 realizations of the FBM series. We summarize the corresponding numerical results in Table I, which includes the Hurst index H, the average box-counting dimension $\langle D(0) \rangle$, the average information dimension $\langle D(1) \rangle$, the average correlation dimension $\langle D(2) \rangle$, and $\Delta D(q)$, where the quantity

$$\Delta D(q) = \max D(q) - \min D(q) \qquad (16)$$

was used to verify how $D(q)$ changes along each curve. From Table I, we can see that the average box-counting dimension $\langle D(0) \rangle$, the average information dimension $\langle D(1) \rangle$, and the average correlation dimension $\langle D(2) \rangle$ roughly decrease with the increase of the Hurst index H from 0.4 to 0.95. We show the average $\langle \tau_1(q) \rangle$ curves in Fig. 13 and average $\langle D(q) \rangle$ curves in Fig. 14. From Figs. 13 and 14, we find that the $\langle \tau_1(q) \rangle$ and $\langle D(q) \rangle$ curves of recurrence networks are not straight lines. So the multifractality exists in these recurrence networks constructed from the FBM series. Meanwhile, we also find that
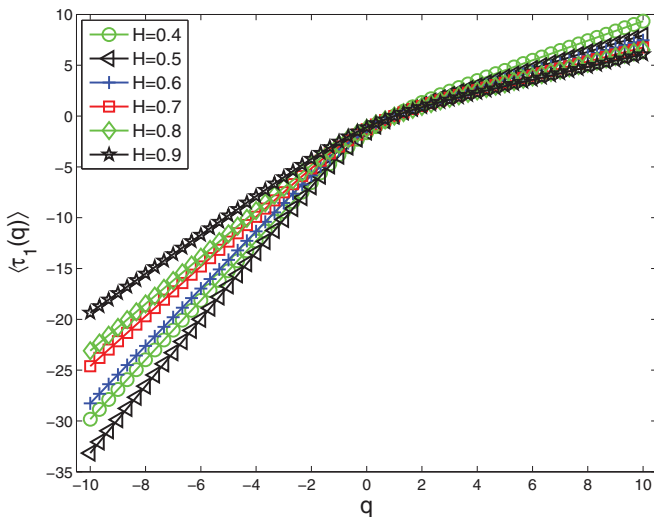

FIG. 13. (Color online) Average $\tau_1(q)$ curves of the recurrence networks. Here the average is calculated from 100 realizations.
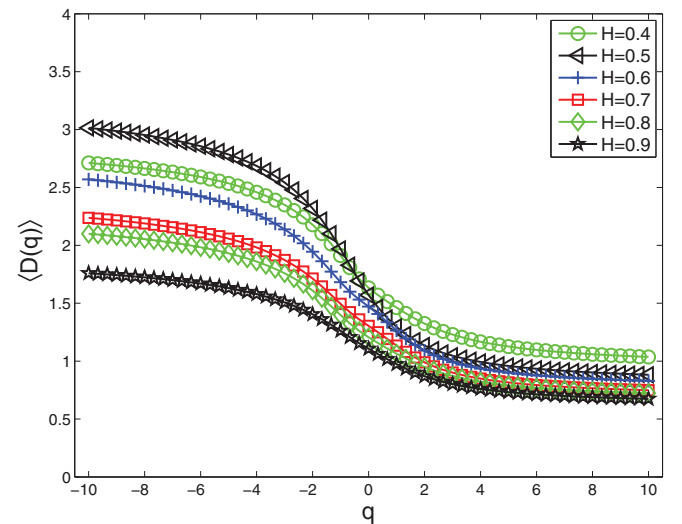

FIG. 14. (Color online) Average $D(q)$ curves of the recurrence networks; $D(0)$ is the fractal dimension of the network. Here the average is calculated from 100 realizations.
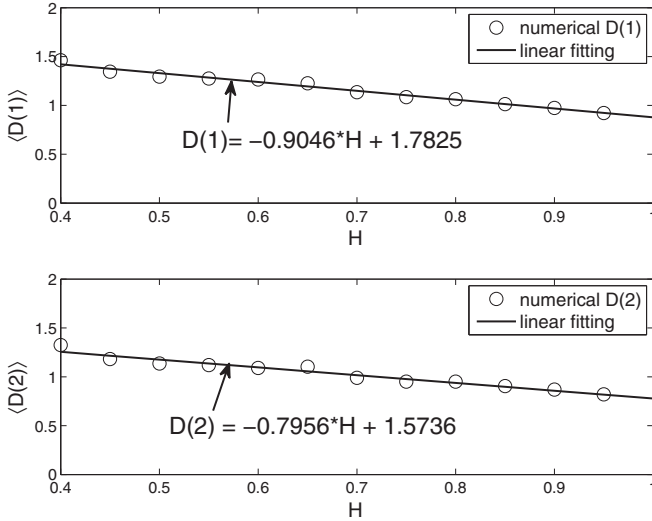
FIG. 15. Dependence of the average information dimension $\langle D(1)\rangle$ and the average correlation dimension $\langle D(2)\rangle$ of the associated recurrence networks with respect to the Hurst index H of fractional Brownian motion. Here the average is calculated from 100 realizations.

the multifractality of these networks becomes stronger at first and then weaker which is indicated by the value of $\Delta D(q) = D(-10) - D(10)$ when the Hurst index of the associated time series becomes larger from 0.4 to 0.95. In particular, the recurrence network with the Hurst index $H = 0.5$ possesses the strongest multifractality. The dependence relationships of the average information dimension $\langle D(1)\rangle$ and the average correlation dimension $\langle D(2)\rangle$ on the Hurst index H are given in Fig. 15. As shown in Fig. 15, we find that these relationships can be well fitted by the following linear formulas:

$$\langle D(1)\rangle = 1.7825 - 0.9046H \tag{17}$$

and

$$\langle D(2)\rangle = 1.5736 - 0.7956H. \tag{18}$$

VI. CONCLUSIONS

In this work, we constructed recurrence networks from FBM series based on the idea of recurrence plot. We extracted the statistical properties of time series from the perspective of complex networks. We studied the basic topological features of the recurrence networks constructed from FBM series with different Hurst indices H. Our numerical results indicate that the recurrence networks constructed exhibit exponential degree distributions. With the increase of H, the average

degree exponent $\langle\lambda\rangle$ increases first and then decreases. The relationship between H and $\langle\lambda\rangle$ can be fitted by a cubic polynomial function. It was found that the average clustering coefficient $\langle C\rangle$ increases with the Hurst index H, which means that there are more transitive and stable structures for networks constructed from FBMs with large Hurst index H. At the microscopic level, we investigated the motif rank distribution of recurrence networks. We found that the recurrence networks are grouped into two superfamilies based on the motif rank distribution. The three key motifs M_1, M_5, and M_6 determine the motif rank pattern and then classify networks. At the same time, we also paid attention to the dependence relationship of the average occurrence frequency $\langle P(M)\rangle$ with respect to the Hurst index H.

From the aspect of fractality and self-similarity, we performed fractal and multifractal analyses using the random sequential box-covering method and the improved method based on a modified fixed-size box-counting algorithm, respectively. The numerical results show that the average fractal dimension $\langle d_B\rangle$ decreases with Hurst index H and the linear relationship $\langle d_B\rangle \approx 2 - H$ was obtained surprisingly. Moreover, our numerical results of multifractal analysis show that the multifractality exists in these recurrence networks, and the multifractality of these networks becomes stronger at first and then weaker when the Hurst index of the associated time series becomes larger from 0.4 to 0.95. In particular, the recurrence network with the Hurst index $H = 0.5$ possesses the strongest multifractality. We also noted that the average information dimension $\langle D(1)\rangle$ and the average correlation dimension $\langle D(2)\rangle$ roughly decrease with the increase of the Hurst index H from 0.4 to 0.95. The dependence relationships of the average information dimension $\langle D(1)\rangle$ and the average correlation dimension $\langle D(2)\rangle$ on the Hurst index H can be well fitted with linear functions. From the above results, we conclude that the inherent nature of time series affects the structure characteristics of the associated networks and the dependence relationship between them appears retained. Our work supports complex network as a suitable and effective tool to perform time series analysis.

[1] R. Albert and A. L. Barabási, Rev. Mod. Phys. **74**, 47 (2002).

[2] R. V. Donner, Y. Zou, J. F. Donges, N. Marwan, and J. Kurths, Phys. Rev. E **81**, 015101(R) (2010).

[3] R. V. Donner, Y. Zou, J. F. Donges, N. Marwan, and J. Kurths, New J. Phys. **12**, 033025 (2010).

[4] D. J. Watts and S. H. Strogatz, Nature (London) **393**, 440 (1998).

[5] A. L. Barabási and R. Albert, Science **286**, 509 (1999).

[6] M. E. J. Newman, SIAM Rev. **45**, 167 (2003).

[7] M. Small, J. Zhang, and X. K. Xu, Lect. Notes Inst. Comput. Sci. Soc. Inf. Telecommun. Eng. **5**, 2078 (2009).

[8] L. Lacasa, B. Luque, F. Ballesteros, J. Luque, and J. C. Nuño, Proc. Natl. Acad. Sci. USA **105**, 4972 (2008).

[9] B. Luque, L. Lacasa, F. Ballesteros, and J. Luque, Phys. Rev. E **80**, 046103 (2009).

[10] C. B. Li, H. Yang, and T. Komatsuzaki, Proc. Natl. Acad. Sci. USA **105**, 536 (2008).

[11] N. Marwan, J. F. Donges, Y. Zou, R. V. Donner, and J. Kurths, Phys. Lett. A **373**, 4246 (2009).

[12] X. K. Xu, J. Zhang, and M. Small, Proc. Natl. Acad. Sci. USA **105**, 19601 (2008).

[13] C. Liu and W. X. Zhou, J. Phys. A **43**, 495005 (2010).

[14] J. P. Eckmann, S. O. Kamphorst, and D. Ruelle, Europhys. Lett. **4**, 973 (1987).

[15] J. P. Zbilut and C. L. Webber, Jr., Phys. Lett. A **171**, 199 (1992).

[16] C. L. Webber, Jr., and J. P. Zbilut, J. Appl. Physiol. **76**, 965 (1994).

[17] TOCSY: http://tocsy.pik-potsdam.de.

[18] J. P. Zbilut, A. Giuliani, and C. L. Webber, Jr., Phys. Lett. A **246**, 122 (1998).

[19] N. Marwan and J. Kurths, Phys. Lett. A **302**, 299 (2002).

[20] M. C. Romano, M. Thiel, J. Kurths, and W. von Bloh, Phys. Lett. A **330**, 214 (2004).

[21] J. F. Donges, J. Heitzig, R. V. Donner, and J. Kurths, Phys. Rev. E **85**, 046105 (2012).

[22] R. V. Donner, J. F. Donges, Y. Zou, N. Marwan, and J. Kurths, in *Proceedings of the 2010 International Symposium on Nonlinear Theory and its Applications NOLTA2010 (Krakow 2010)* (IEICE, Tokyo, 2010), pp. 87–90.

[23] B. B. Mandelbrot and J. W. Van Ness, SIAM Rev. **10**, 422 (1968).

[24] L. Lacasa, B. Luque, J. Luque, and J. C. Nuño, Europhys. Lett. **86**, 30001 (2009).

[25] W. J. Xie and W. X. Zhou, Physica A **390**, 3592 (2011).

[26] Y. Zhou, Y. Leung, and Z. G. Yu, Phys. Rev. E **87**, 012921 (2013).

[27] M. A. Riley, R. Balasubramaniam, and M. T. Turvey, Gait Posture **9**, 65 (1999).

[28] J. S. Kim, K. I. Goh, G. Salvi, E. Oh, B. Kahng, and D. Kim, Phys. Rev. E **75**, 016110 (2007).

[29] B. G. Li, Z. G. Yu, and Y. Zhou, J. Stat. Mech.: Theor. Exp. (2014) P02020.

[30] D. L. Wang, Z. G. Yu, and V. Anh, Chin. Phys. B **21**, 080504 (2012).

[31] N. H. Packard, J. P. Crutchfield, J. D. Farmer, and R. S. Shaw, Phys. Rev. Lett. **45**, 712 (1980).

[32] F. Takens, in *Dynamical Systems and Turbulence*, edited by D. A. Rand and L. S. Young, Lecture Notes in Mathematics (Springer-Verlag, Berlin, 1981), Vol. 898, p. 366.

[33] M. Casdagli, S. Eubank, J. D. Farmer, and J. Gibson, Physica D **51**, 52 (1991).

[34] M. T. Rosenstein, J. J. Collins, and C. J. De Luca, Physica D **73**, 82 (1994).

[35] A. M. Fraser and H. L. Swinney, Phys. Rev. A **33**, 1134 (1986).

[36] M. B. Kennel, R. Brown, and H. D. I. Abarbanel, Phys. Rev. A **45**, 3403 (1992).

[37] L. Y. Cao, Physica D **110**, 43 (1997).

[38] N. Marwan, M. C. Romano, M. Thiel, and J. Kurths, Phys. Rep. **438**, 237 (2007).

[39] M. A. Riley and G. C. Van Orden, *Tutorials in contemporary nonlinear methods for the behavioral sciences*, http://www.nsf.gov/sbe/bcs/pac/nmbs/nmbs.jsp.

[40] P. Erdős and A. Rényi, Publ. Math. Debrecen **6**, 290 (1959).

[41] M. S. Roulston, Physica D **125**, 285 (1999).

[42] Z. H. Tang and Z. G. Yu, Chin. J. Eng. Math. **29**, 499 (2012).

[43] D. F. Gleich, *A graph library for Matlab based on the boost graph library*, http://dgleich.github.com/matlab-bgl.

[44] http://pajek.imfm.si/doku.php?id=pajek.

[45] A.-L. Barabási and E. Bonabeau, Sci. Am. **288**, 60 (2003).

[46] X. H. Ni, Z. Q. Jiang, and W. X. Zhou, Phys. Lett. A **373**, 3822 (2009).

[47] R. Milo, S. S. Orr, S. Itzkovitz, N. Kashtan, D. Chklovskii, and U. Alon, Science **298**, 824 (2002).

[48] R. Milo, S. Itzkovitz, N. Kashtan, R. Levitt, S. S. Orr, I. Ayzenshtat, M. Sheffer, and U. Alon, Science **303**, 1538 (2004).

[49] http://www.weizmann.ac.il/mcb/UriAlon/.

[50] B. B. Mandelbrot, Science **156**, 636 (1967).

[51] J. Feder, *Fractals* (Plenum, New York, 1988).

[52] B. B. Mandelbrot, *The Fractal Geometry of Nature* (Academic, New York, 1983).

[53] G. Palla, I. Derenyi, I. Farkas, and T. Vicsek, Nature (London) **435**, 814 (2005).

[54] K. I. Goh, G. Salvi, B. Kahng, and D. Kim, Phys. Rev. Lett. **96**, 018701 (2006).

[55] C. Song, S. Havlin, and H. A. Makse, Nature (London) **433**, 392 (2005).

[56] C. Song, L. K. Gallos, S. Havlin, and H. A. Makse, J. Stat. Mech.: Theor. Exp. (2007) P03006.

[57] W. X. Zhou, Z. Q. Jiang, and D. Sornette, Physica A **375**, 741 (2007).

[58] R. W. Floyd, Commun. ACM **5**, 345 (1962).

[59] R. V. Donner, J. Heitzig, J. F. Donges, Y. Zou, N. Marwan, and J. Kurths, Eur. Phys. J. B **84**, 653 (2011).

[60] E. Canessa, J. Phys. A: Math. Gen. **33**, 3637 (2000).

[61] V. V. Anh, Q. M. Tieng, and Y. K. Tse, Int. Trans. Oper. Res. **7**, 349 (2000).

[62] Z. G. Yu, V. Anh, and K. S. Lau, Phys. Rev. E **64**, 031903 (2001).

[63] Z. G. Yu, V. Anh, and K. S. Lau, Phys. Rev. E **68**, 021913 (2003).

[64] Z. G. Yu, V. Anh, and K. S. Lau, J. Theor. Biol. **226**, 341 (2004).

[65] Z. G. Yu, V. V. Anh, K. S. Lau, and L.Q. Zhou, Phys. Rev. E **73**, 031920 (2006).

[66] Z. G. Yu, V. Anh, and R. Eastes, J. Geophys. Res. **114**, A05214 (2009).

[67] Z. G. Yu, V. Anh, Y. Wang, D. Mao, and J. Wanliss, J. Geophys. Res. **115**, A10219 (2010).

[68] T. C. Halsey, M. H. Jensen, L. P. Kadanoff, I. Procaccia, and B. I. Shraiman, Phys. Rev. A **33**, 1141 (1986).